THE INFLUENCE OF GEOMETRIC SIMPLIFICATIONS OF AN AIRCRAFT WITH RESPECT TO THE OPTIMIZATION OF THE AERODYNAMIC CHARACTERISTICS OF THE VERTICAL TAILPLANE

A. Kröhnert, German Aerospace Center (DLR), Aerodynamics and Flow Technology,
Lilienthalplatz 7, 38108 Braunschweig, Germany
L. Gebhardt, Airbus Operations GmbH, Aerodynamics Domain,
Airbus-Allee 1, 28199 Bremen, Germany

Abstract

Having as long-term strategy the multi-disciplinary optimization of the vertical tailplane (VTP) of a conventional transport aircraft in mind, some basic studies targeting the aerodynamic analysis were conducted as part of a cooperative project between Airbus and DLR. A first study in this context, which was carried out as part of the AeroNext research project, led to the conclusion, that due to the complexity of the flow around the VTP caused by the flow conditions at the identified design cases and its main geometric characteristics (low aspect ratio and high sweep), at least 3d RANS methods are required to capture all relevant flow-physical effects. Because 3d-RANS-methods are still expensive when considering them as analysis method for a numerical optimization, other ways were sought after to decrease the computational time required for each analysis. Therefore an assessment was carried out to decide whether one would obtain the same optimization result when performing the optimization with the VTP on the complete aircraft geometry compared to an optimization where parts or even everything but the VTP is removed in order to reduce time and cost for mesh generation and flow analysis. This was checked using two different VTP geometries in combination with four different simplification levels of the aircraft. One set of VTP characteristics was derived from each of those simplification levels by calculating different coefficients and gradients for low and high speed flight conditions, believed to be a necessary part of the objective function required for an actual optimization. In order to understand the differences in the VTP characteristics obtained for the different simplification levels, the effects which lead to the changes in the aerodynamic behavior are discussed. The numbers obtained for the two exemplary VTPs alone do not deliver final proof that any considerable simplification will lead to a different optimization result. However, the fact that the differences between the configurations vary in magnitude between the two VTPs, compounded by the very different local flow conditions found on and around the VTP depending on the configurations and onset flow conditions, leads to the conclusion, that it is in general not advisable to heavily simplify the configuration to be optimized unless robust knowledge about the characteristics of the objective function is available in order to avoid detrimental effects on the optimization result obtained.

1. INTRODUCTION

1.1. Background and Motivation

A cooperative project between DLR and Airbus is part of a long-term strategy to improve the tails of a conventional transport aircraft configuration by means of numerical optimization in a multi-disciplinary context. A stepping stone of turning that strategy into reality is the optimization of the aerodynamic characteristics of the vertical tailplane (VTP). With the challenges of a practical application of numerical optimization in mind, described in a bit more detail further below, the investigation presented in this paper was started.

The VTP's main task is to provide stability and control for the aircraft about the yaw axis. It houses no passengers, freight or fuel. Therefore, in a multi-disciplinary context, its influence on the NRC (Non Recurring Costs) and DOC (Direct Operating Costs) should be as low as possible, resulting from selecting the best compromise among others between size, weight, manufacturing cost, maintenance cost, and drag. The aerodynamic objective alone is of course to design a VTP which fulfils its role with regard to stability and control under all required conditions while creating the lowest drag possible during cruise flight.

Under normal operating conditions without strong gusts or crosswinds and if just small changes in the heading of the aircraft are required, the VTP only needs to create a relatively small side force, especially during cruise flight. Here the flow velocity is quite high requiring only small deflections to produce the same force as for lower flight velocities. However, for some cases like strong crosswinds or a malfunction of one engine during start or landing or if a very fast reaction time of the aircraft is needed for a sudden maneuver, for example in the case of a gust encounter, a high side force resp. side force gradient has to be generated by the VTP. While it is of course required to take such cases into account during the design of the VTP it is also obvious that those cases lead to a larger VTP, consequently higher weight, more wetted area and therefore also drag.

Due to the competing requirements it is quite challenging to find an optimal solution for the design of the VTP. For the overall design of the aircraft it is of course not sufficient to optimize only the aerodynamic characteristics. Also, as initially mentioned, other factors like weight, manufacturing and maintenance cost and many others have an influence on the optimum VTP, leading to the consequence that a multi-disciplinary approach will be needed in order to find an optimum solution at aircraft level in the end. The concentration on the aerodynamic effects as done in the

remainder of this paper thus can only be seen as a first step in trying to understand the effects in this single domain.

One possible way to find an optimum VTP design is the use of numerical optimization using dedicated mathematical algorithms. While such an approach is not suitable by any means to replace the experience and knowledge of a good aerodynamicist, it can serve as a vehicle to find new and especially unconventional solutions for complex problems. One well known drawback of numerical optimization is that the algorithms react only to a limited set of quantities, expressed in terms of objective function and constraints, which may only partially describe the whole complexity of the design problem. From that aspect, the algorithms may steer the search procedure to an unwanted area if the modeling used presents a weakness leading to an "artificial" improvement of the goal function. For example, with regard to the VTP, an investigation using a two-dimensional airfoil and an infinite swept wing gave no satisfactory agreement compared to the results of a three-dimensional (3d) VTP computation [1]. Due to the low aspect ratio and high sweep angle of the VTP of a conventional jet transport aircraft, 3d effects are quite pronounced and a 2d or 2.5d modeling has proven insufficient to capture the relevant aspects of the problem. Thus, after considering the experiences from the previous study and the most important design cases of the VTP, it was decided that a new approach using three-dimensional modeling in combination with high-fidelity tools is required. Due to the demanding aerodynamic flow conditions prevalent at the VTP design cases involving considerable areas of separated flow, RANS-methods (Reynolds-averaged Navier-Stokes methods) were selected as the minimum necessary representation of the problem at hand, hopefully still giving robust and meaningful results under such conditions.

However, RANS-methods are still very expensive when considering them as analysis method for numerical optimization, especially for demanding flow conditions and the quite refined computational meshes required to study them. Thus it was decided to investigate possibilities to reduce the time and cost needed by decreasing the complexity of the aircraft geometry. In order to get an answer to the question what kind of simplifications are permissible, the effects on the characteristics of the VTP have to be assessed. With the intent of performing a numerical optimization, the question to be answered is: "What is the effect of the simplification on the optimization result?" Or in other words: Will a different VTP design result from the optimization due to the simplification, which then would no longer be optimal for the actual, complete aircraft configuration?

1.2. Scope

The VTP is usually not as much in the focus of research efforts as for example the wing. Thus data or even a complete consistent investigation on the influence of the other aircraft components on the VTP is not available. The consistency between the calculations, however, is of utmost importance to capture the influence between the components and also small effects which can else arise from other differences in the setup or the geometry. In addition, the role of the VTP or HTP differs from that of the wing concerning the magnitude of the effect other aircraft components have on them, simply due to their location downstream at the rear part of the aircraft.

At the beginning of this investigation to quantify the impact of simplifying the aircraft geometry on the VTP characteristics some data was obtained for an initial VTP design. These first results were published in [2]. In the present paper the results are extended to a second VTP design, which allows drawing some conclusions regarding the impact one could anticipate for a VTP optimization. Also, the aerodynamic effects leading to the results obtained are discussed in more detail.

2. INVESTIGATION APPROACH AND METHODS

In the following paragraphs the geometry cases selected for the investigation and the flight conditions used for the calculations are described. Further more, it is explained which gradients and coefficients are used to determine the VTP characteristics and how they are calculated. Some information about the geometry used, the mesh generation, and the flow calculations are given as well.

2.1. Selection of Configurations and Flight Cases

For the systematic investigation, similar to the analysis presented in [2], the VTP characteristics were investigated as resulting from different levels of geometric simplification of the aircraft:

1) VTP calculated on a symmetry plane which corresponds to an infinite inviscid plate (VTP on sym. plane)
2) VTP on a fuselage (VTP+fus)
3) VTP with horizontal tailplane (HTP) and fuselage (VTP+HTP+fus)
4) VTP with HTP, wing, belly fairing and fuselage (VTP+HTP+wing+belly+fus)

The resulting geometries are visualized in Fig. 1.

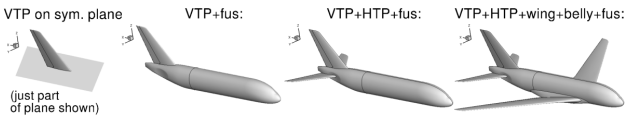

Fig. 1. Overview of the four different geometry configurations investigated

For each of the four simplification levels a set of calculations was carried out for different flow conditions and flight cases. Selected were those which have the most determining influence on the aerodynamic design of the VTP. The flow conditions chosen and the corresponding Reynolds numbers related to the mean aerodynamic chord (MAC) of the wing are:

– Low Speed (LS):
  M = 0.2, Altitude: 0ft/0m, Re = 53.62 · 10^6 at l_{ref} = 11.509m (≙MAC_{Wing})

– High Speed (HS):
  M = 0.85, Altitude: 35000ft/10668m, Re = 76.82 · 10^6
  at l_{ref} = 11.509m (≙MAC_{Wing})

Those two different flight conditions are combined with different angles of sideslip β and rudder deflection δ_r to arrive at the cases analyzed for each configuration. From the calculated results the following coefficients and gradients can be determined to describe the main characteristics of the VTP:

– $C_{YV,OEI-DC}$: Side force coefficient for simulated One-Engine-Inoperative (OEI) design case (DC) (see Fig. 2) at LS conditions (maximum rudder deflection (δ_r = −35°) with small sideslip angle (β = 5°), leading to large areas of separated flow on the VTP)
– $C_{Y\delta r}$: Change of side force coefficient due to change in rudder deflection angle (δ_r linear range, β = 0°), also called rudder efficiency, at LS and HS conditions.
– $C_{YV\beta}$: Change of side force coefficient of the VTP due to change in sideslip angle (β linear range, δ_r = 0°), also called VTP efficiency, at LS and HS conditions.
– $C_{DV,HS}$: Drag coefficient of the VTP at HS (cruise) conditions (β = 0°, δ_r = 0°). In cruise flight the VTP must provide the required stability at minimum drag. Thus small differences in VTP cruise drag have to be captured reliably.

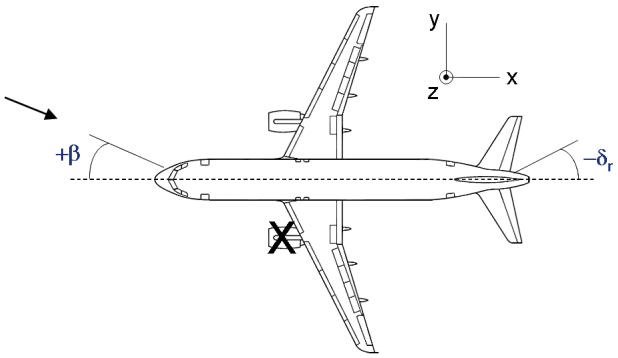

Fig. 2. One Engine Inoperative maneuver with sideslip and rudder deflection angle definition

The results of the simplified configurations are compared to those of the most complete one as reference case. The angle of attack for all calculations is set to zero for reasons of comparability since the VTP on the symmetry plane can be investigated for zero angle of attack only. The incidence angle i_H of the horizontal tailplane (HTP) is also kept constant at i_H = 0°, again for reasons of comparability.

The matrix of calculations needed to cover the analysis cases described above was computed for two different VTP planforms (see Fig. 3) in order to assess how the different levels of simplification interact with different VTP geometries. The modification in the planform of the second VTP is resulting from a change of the sweep angle:

– VTP01: Quarter chord sweep angle ϕ_{25} = 40°
– VTP02: Quarter chord sweep angle ϕ_{25} = 35°

The reduction of the VTP sweep angle should lead to an increase of the non-linear aerodynamic effects making them more visible in the results.

2.2. CAD-Model

The geometry used for the investigation is the Megaliner transport aircraft research configuration X55D which was already the model of choice in several European research projects like REMFI (Rear Fuselage and Empennage Flow Investigation) [3][4][5].

To obtain the different rudder deflections and VTP designs the geometry was parameterized using the commercial CAD (Computer-Aided Design) program CATIA V5 (Computer Aided Three-Dimensional Interactive Application) from Dassault Systèmes.

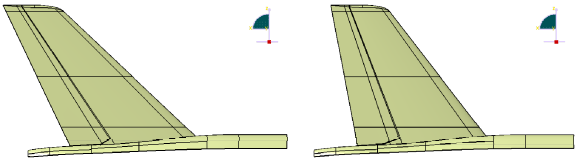

Fig. 3. Geometry of the VTP's (left: VTP01, right: VTP02)

2.3. Computational Mesh

The mesh generation was conducted with the commercial mesh generation package CENTAUR from CentaurSoft [6]. It produces hybrid grids consisting of a mixture of prisms, hexahedra, tetrahedra and pyramids. The version used was 8.1.4.

A major objective during the mesh generation was to keep the mesh quality as similar as possible between the simplified configurations and VTP planforms as well as between the Reynolds numbers and rudder deflections. To accomplish this, a consistent meshing strategy is applied for all meshes. This ensures not only very similar meshes but also allows a better comparison between the cases and configurations due to as constant mesh effects as possible on the results.

The farfield was extended about 20 times the half wing span to each side of the aircraft. The discretization of lifting surfaces is done in such a way that every airfoil has a basic resolution of about 100 cells per chord. This resolution is the same for each airfoil and independent of its actual chord length. At the leading and trailing edge the cells are further refined as is done in general in areas with small geometrical details or high flow gradients as well as in intersection areas between components.

The approximate number of nodes obtained for the four different configurations is given in TAB 1 and is the same independent of the VTP planform.

For the second set of calculations using VTP02 a modular meshing approach was introduced to reduce the meshing time. Therefore a box was constructed in CATIA around the VTP. Now, after the whole mesh has been created once, only the part inside the box has to be re-meshed if for example the rudder deflection changes. Compared to VTP01 only at two locations some small changes in the source settings were necessary when the box was

introduced, which allowed to keep the meshes as similar as possible.

Configuration	approx. total points	approx. TAU calc. time [h], old/new cluster
VTP on symmetry plane	5 000 000	19/08
VTP+fus	10 000 000	37/15
VTP+HTP+fus	20 000 000	66/25
VTP+HTP+wing+belly +fus	40 000 000	99/46

TAB 1. Number of nodes and resulting wallclock time needed for TAU runs using 64 CPUs (cores)

2.4. Flow Calculation

The flow computations were carried out with the unstructured flow solver TAU release 2008.1.1, developed mainly by the DLR [7][8]. All calculations were run on the $C^2A^2S^2E$ (Center for Computer Applications in AeroSpace Science and Engineering) cluster located at the DLR site (Deutsches Zentrum für Luft- und Raumfahrt – German Aerospace Center) in Braunschweig.

The viscous, fully turbulent calculations were performed using the turbulence model of Spalart and Allmaras with the modification introduced by Edwards. The temporal discretization is realized by an implicit Backward-Euler scheme with the linear LUSGS (Lower-Upper Symmetric Gauss-Seidel) solver. The inviscid flux discretization type for the first stage of 1000 iterations is a first order upwind scheme, thereafter switching to the central scheme introduced by Jameson. For convergence acceleration a 3w multigrid scheme is used. For the configuration consisting of the isolated VTP a symmetry boundary condition is used to simulate the infinite inviscid base plate.

All calculations from which data is presented here are sufficiently converged. For monotonous convergence behavior the main criterion for convergence is the change in the drag coefficient which should be 10^{-6} or smaller during the last 500 iterations. For an oscillatory convergence behavior of the coefficients of lift, drag and side force, the individual mean value of each of the last couple of periods should be identical and the amplitude of the oscillation must be small compared to the mean value of the oscillation. The approximate wallclock time needed for the four different configurations is given in TAB 1, assuming that 64 CPUs (nodes) are used for each calculation and each calculation is run for 30000 iterations. Between the calculation of the two geometries VTP01 and VTP02 the cluster was upgraded to increase its performance. That reduced the calculation time on average by about a bit more than half when using the same settings and number of nodes as before.

2.5. Analysis Approach

In this section it is explained how the coefficients and gradients which were selected to describe the VTP characteristics are determined.

2.5.1. Side Force Coefficient for Simulated One-Engine-Inoperative Design Case

For the purposes of this paper, the One-Engine-Inoperative (OEI) design case is defined as the case, when maximum rudder deflection is combined with a small sideslip angle, which is usually applied together with the allowed small bank angle to support the VTP [9]. This high rudder deflection angle is required to counteract the yawing moment arising due to the loss of thrust in one engine at low airspeeds, for example right after take-off when the thrust of the remaining engine inducing the yawing moment is very high.

To calculate the coefficient $C_{YV,OEI\text{-}DC}$ two calculations are necessary to isolate the value of the side force coefficient produced by the VTP (C_{YV}). The first calculation is the respective configuration where the tails, i. e. the VTP and the HTP, are included. The word tail on the other hand would just mean the HTP. The second calculation comprises the same configuration but without the VTP and, for the configurations where it exists, the HTP. The side force coefficient generated by the VTP is then obtained by subtracting the side force coefficient of the second calculation from the one of the first calculation:

$$C_{YV,OEI-DC} = C_V\left(Tails\ \ on, \beta = 5^\circ, \delta_r = -35^\circ\right) - C_V\left(Tails\ \ off, \beta = 5^\circ\right) \quad (1)$$

In the preceding paragraph it was stated that “Tails off” means that VTP and HTP are removed from the geometry. As can be seen from Eq. (1), the calculation to be subtracted is a Tails-off configuration. The reasoning behind removing not only the VTP but also the HTP in order to isolate the side force coefficient generated by the VTP is found partially in the fact that the HTP is trimmable. Would the HTP be left on the configuration, a trim-setting dependent C_{YV} would result, complicating the description of the aircraft characteristics.

2.5.2. Change of Side Force Coefficient due to Change in Rudder Deflection

To obtain the gradient $C_{Y\delta r}$ the linear part of the C_Y versus δ_r curve is of interest. Therefore only small rudder deflections are applied. The two rudder deflection angles selected here are $\delta_r = 0°$ and $\delta_r = -2°$. Because the onset flow is symmetric to the airplane (x-z-plane) and the airplane itself is symmetric as well, the side force for the case with $\delta_r = 0°$ is zero since the VTP without rudder deflection has a symmetric airfoil. Thus just the calculation for the case with $\delta_r = -2°$ is required. The rudder efficiency is then determined by:

$$C_{Y\delta r} = \frac{C_Y\left(\delta_r = 0^\circ\right) - C_Y\left(\delta_r = -2^\circ\right)}{\left(\delta_r = 0^\circ\right) - \left(\delta_r = -2^\circ\right)} = \frac{C_Y\left(\delta_r = -2^\circ\right)}{2^\circ} \quad (2)$$

The coefficient C_Y here shall only represent the

contribution of the VTP caused by the rudder deflection. To separate this effect from the C_Y induced by the rest of the geometry like the fuselage, two calculations would be necessary, similar to the calculation of the coefficient $C_{YV,OEI\text{-}DC}$ where a tails-off configuration was subtracted from a tails-on configuration. Since now the rudder deflection is of interest this would correspond here to the calculation with zero rudder deflection being subtracted from a calculation where the configuration has non-zero rudder deflection. Because the aircraft is symmetric, the side force contribution of the case with δ_r = 0° would be zero for the symmetric flow conditions applied here. Thus no such calculation needs to be performed to obtain the coefficient C_Y which in turn is used to calculate the gradient $C_{Y\delta r}$. If the aircraft would be asymmetric, i. e. $C_Y(\delta_r = 0) \neq 0$, such a calculation with zero rudder deflection would have to be performed additionally to the ones mentioned above for Eq. (2).

2.5.3. Change of Side Force Coefficient due to Change in Sideslip Angle

The gradient $C_{YV\beta}$ is obtained similar to $C_{Y\delta r}$ described above with the difference that the rudder deflection angle δ_r is exchanged with the sideslip angle β. The sideslip angles chosen for the calculation of the gradient are β = 0° and β = 2°. The definition of the sign of the sideslip angle is shown in Fig. 2. Here for the case with β = 0° symmetric flow conditions are present and because of the symmetric geometry the side force generated is zero. Thus just the calculation for the case with β = 2° is required. The VTP efficiency is determined by:

$$C_{YV\beta} = \frac{C_{YV}(\beta = 0^\circ) - C_{YV}(\beta = 2^\circ)}{(\beta = 0^\circ) - (\beta = 2^\circ)} = \frac{C_{YV}(\beta = 2^\circ)}{2^\circ} \tag{3}$$

C_{YV} itself is obtained as follows (corresponding to Eq. (1)):

$$C_{YV} = C_Y(Tails\ on) - C_Y(Tails\ off) \tag{4}$$

2.5.4. Drag Coefficient of the VTP at Cruise Flight Conditions

For the calculation of $C_{DV,HS}$ zero rudder deflection angle and zero sideslip angle are selected. The load on the VTP in cruise flight is usually very small and just small sideslip angles and rudder deflections occur. The determination of the drag is done in accordance with the way this is done for wind tunnel experiments.

Because the drag of the VTP is already rather small (usually in the range of 10 to 12 drag counts (1 drag count (dc) $\triangleq 1 \cdot 10^{-4}$) at cruise conditions), it is not easy to determine the change in drag due to a modification of the VTP geometry reliably. Because the HTP is a movable part of the aircraft, the drag it produces is dependent on its incidence angle i_H. Furthermore this incidence angle has also an influence on the VTP and the flow around it. Therefore the drag produced by the VTP is determined without the HTP on the airplane. For the full configuration with VTP+HTP+wing+belly+fus the VTP drag would be calculated by:

$$C_{DV,HS} = C_D(VTP + wing + belly + fus) - C_D(wing + belly + fus) \tag{5}$$

3. RESULTS: INFLUENCE OF THE GEOMETRIC DIFFERENCES ON THE AERODYNAMIC CHARACTERISTICS OF THE VTP

In this chapter general aerodynamic observations and effects are discussed which can be found when looking for example at pressure coefficient (c_p) distributions. The link to the coefficients and gradients described above is explained in the next chapter.

3.1. Sectional Pressure Coefficient Distributions

In Fig. 4 the pressure section locations together with their dimensionless VTP spanwise coordinate η, for which the c_p-distribution will be shown later, are illustrated. The VTP on the symmetry plane has an additional fin area at the root where the VTP planform, normally cut by the curved fuselage, was extended to end at $z_{Fin,min}$ = constant. The increased area is accounted for when calculating the coefficients to allow a more meaningful comparison. For the VTPs on the fuselage the first cut DV1 does not go through the very front of the fin but intersects there with the fuselage.

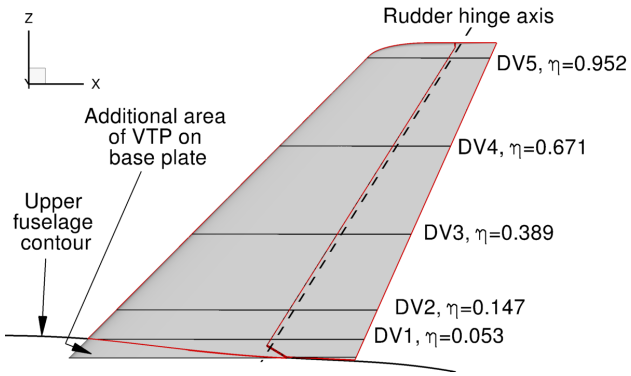

Fig. 4. Pressure section locations along the VTP span

3.1.1. General Effects of Geometry Simplification

For the streamwise VTP cut sections described above the pressure coefficient distribution will now be discussed. As an example to describe the basic effects which can be found, the flight case with δ_r = 0° and β = 2° for VTP02 is used. In Fig. 5 a comparison of the results for the different geometric configurations is shown for M = 0.2. In Fig. 6 the same is depicted for M = 0.85.

The general differences between these two figures result from the transonic effects which the VTP experiences for the high speed flight case at a Mach number of 0.85. The transonic effects change the characteristics of the pressure coefficient distributions compared to the low speed flight case at a Mach number of 0.2 with subsonic behavior. The effects applicable for both subsonic and transonic pressure coefficient distribution are described in this section. After that the results requiring a distinction between the subsonic and the transonic case are discussed in two separate sections.

In Fig. 5 and Fig. 6 it can be observed that the main differences are found in the sections near the VTP root. Towards the tip the c_p-distributions become more alike and only smaller differences can be detected between the configurations. The most noticeable difference exists between all configurations which include the fuselage and the configuration VTP on symmetry plane near the root of the VTP. This can be explained by the different geometry resulting there for this configuration and the modified flow behavior at the VTP. In Fig. 4 it can be seen that due to the spanwise location of the lowest pressure cut section, the cut through the VTP is not complete and instead extends into the fuselage. This also explains why the pressure coefficient distribution for the configurations with fuselage shown for the first pressure section does not start at the leading edge or at the dimensionless chord value of $\eta = 0$. The resulting effect in the c_p-distribution is still visible in the second cut at about 15% of the VTP span. Just the configuration without fuselage has an uncut VTP nose, leading to a pressure distribution more similar to that of the other pressure cut sections.

Due to this incomplete VTP section for the configurations with fuselage, no leading edge of the VTP exists in this section and the flow transitions from the fuselage to the VTP instead. Consequently no stagnation point exists where the normal flow component is decelerated to zero. The flow just meets the VTP at a shallow angle. After that, the acceleration is lower compared to the acceleration from near zero velocity which would otherwise occur. Due to this, no pressure peak occurs at the leading edge at DV1 for the configurations with fuselage. The gradient of the increase towards negative pressure coefficients is smaller compared to the configuration without fuselage and decays faster.

Another important effect is the end plate effect. Adding an end plate increases, for constant geometric aspect ratio, the aerodynamic or effective aspect ratio by impeding the pressure exchange between lower and upper side of a lifting surface, moving the tip vortex further outward. The aerodynamic aspect ratio is thereby calculated using the distance between the tip vortices in place of the geometric span used to determine the geometric aspect ratio. Increasing the aerodynamic aspect ratio leads to an increase in the lift curve slope. In addition, the induced angle of attack is reduced due to the effect of the end plate, increasing the effective angle of attack and consequently the lift or side force produced at a specific angle.

For the VTP on the symmetry plane this plane can be seen as an infinite end plate the effects of which are for example described in [10]. Due to this symmetry plane the geometric aspect ratio is increased by a factor of two. For the VTP on the fuselage there is just a small end plate effect because the fuselage dimensions are much smaller than those of the theoretically infinite symmetry plane. By adding the HTP to the fuselage, the end plate effect is increased again. Thus the addition of the HTP increases the pressure difference between suction and pressure side of the VTP, allowing a higher side force to be produced by the VTP.

Additionally, when comparing the calculation on the symmetry plane and the ones with a fuselage it has to be borne in mind, that on the fuselage a boundary layer develops which does not on the symmetry plane. Inside the boundary layer the flow velocity is reduced towards zero directly on the wall. Since the VTP is located at the rear end of the fuselage, the boundary layer has a considerable thickness, which is about half a meter at the considered low angle of attack. The area of the VTP affected by this is relatively large because the root chord is relatively long. Due to the decelerated flow in this region the force produced there is not as high as it is for the VTP on the symmetry plane where the onset flow in the root area is not disturbed by the boundary layer of the fuselage.

In general it can be concluded that the more the aircraft geometry is simplified the more the pressure distribution varies from that of the complete configuration.

3.1.2. Subsonic Case (M=0.2)

Looking at Fig. 5 the four configurations are in general very similar concerning their c_p-distribution except for the already mentioned difference in the two lowest cuts between the configuration VTP on symmetry plane and all others. Apart from that, the configuration VTP+fus deviates most, noticeable especially in the rear 60% of the chord. However, for the subsonic case the differences are still relatively small. In Fig. 5 it can be observed that these differences can be found especially in the two sections towards the root (DV1 and DV2). Here, the above mentioned end plate effect comes into play, where the missing HTP for the configuration VTP+fus reduces the pressure difference to be found especially for the aft part of the airfoils behind the point of greatest thickness. In x- or streamwise direction the appearance of this difference coincides approximately with the location of the HTP leading edge as can be seen in Fig. 15 or Fig. 16.

The position of maximum thickness moves from root to tip of the VTP from 34.6% to 40.7%. A further aft located position of the maximum thickness leads, as can be seen for example in [11], to a further downstream location of the point of the highest negative pressure. For the subsonic flight case the position of maximum thickness and the minimum pressure coefficient approximately coincide as the flow is accelerated about up to this point. In addition, a further aft located position of the maximum thickness leads to a decreased nose radius if the airfoil is not further modified. A smaller nose radius increases the negative pressure coefficient at the leading edge yielding a higher pressure peak which is clearly noticeable in the pressure distributions of the different cuts.

3.1.3. Transonic Case (M=0.85)

Similar to the subsonic case the pressure coefficient distribution differs most in section DV1. In general the differences are more obvious between the configurations. The geometry simplification has quite a profound effect at transonic flow conditions, attributable to the higher sensitivity of the pressure coefficient distribution to small changes in the flow or the geometry. This is especially noticeable in the root region of the VTP, where replacing the fuselage with a symmetry plane leads to a completely different characteristic of the pressure distribution when compared to the full configuration. In a similar way, although to a smaller extent, this is true for the omission

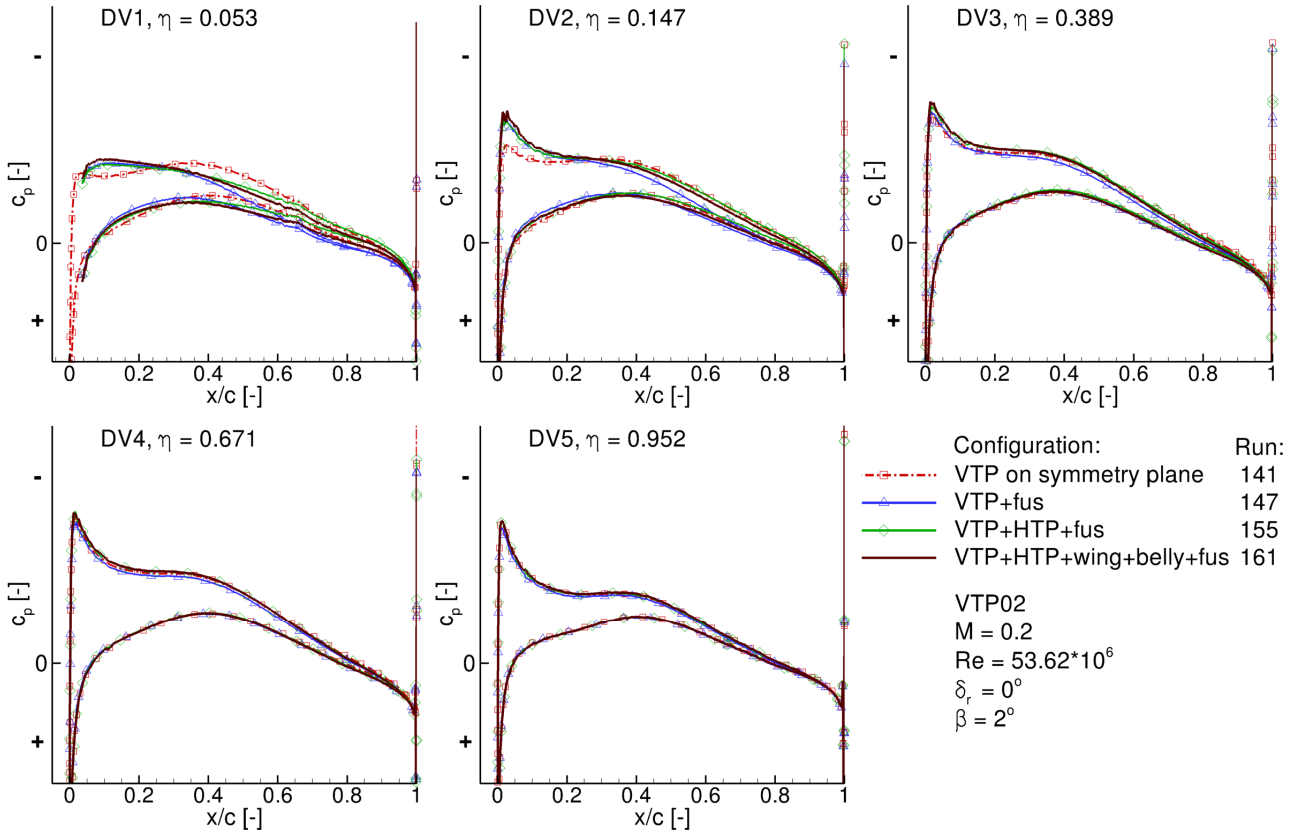

Fig. 5. Pressure coefficient distribution in VTP sections; comparison of the different configurations, $\delta_r = 0°$, $\beta = 2°$, M = 0.2, VTP02

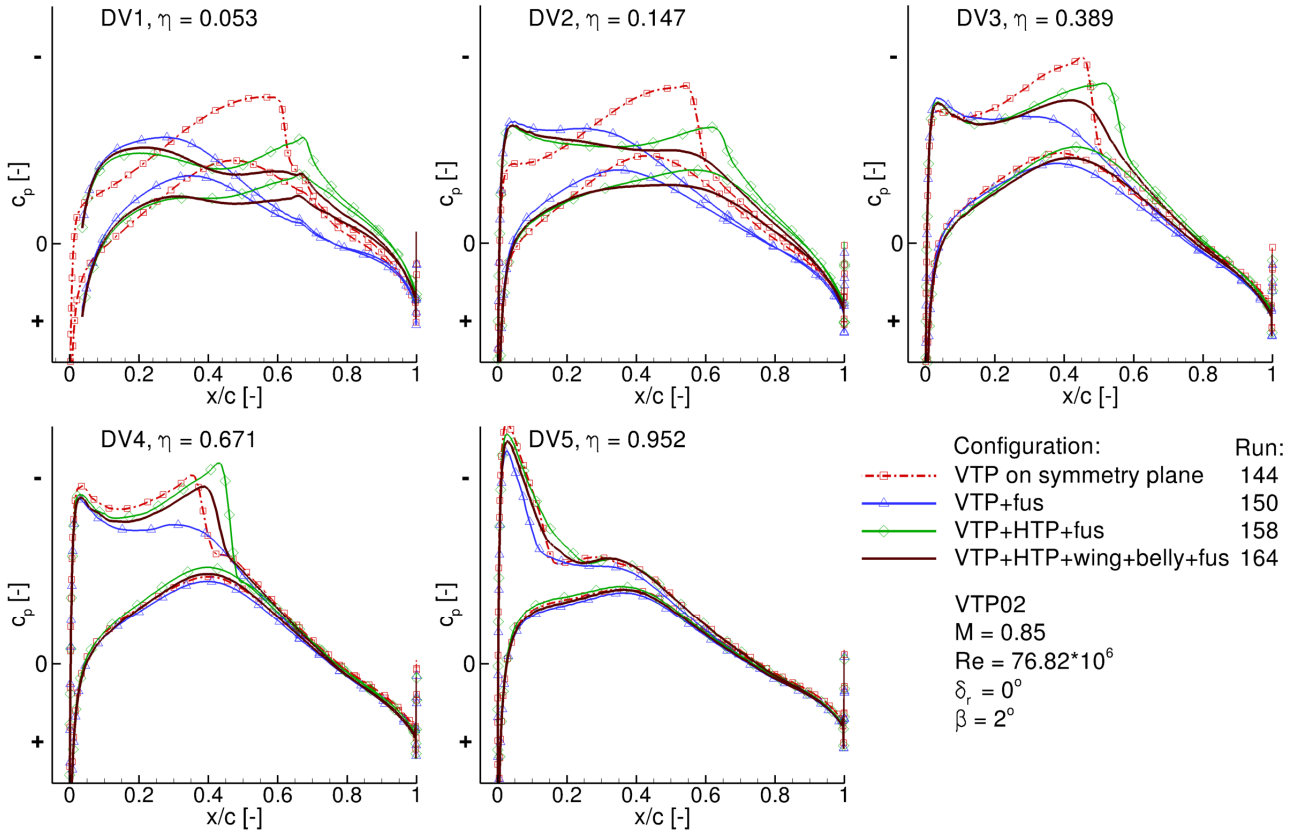

Fig. 6. Pressure coefficient distribution in VTP sections; comparison of the different configurations, $\delta_r = 0°$, $\beta = 2°$, M = 0.85, VTP02

of the HTP. The resulting differences diminish when approaching the VTP tip, but the small differences in the flow due to the geometric differences between the configurations are, even at η = 0.67, sufficient for the presence or non-presence of a shock as can be seen in DV4 in Fig. 6.

The already described effects of the further downstream moved position of maximum thickness can be observed for the transonic cases equally to the subsonic ones. However, here the position of maximum thickness and minimum pressure coefficient are not that directly coupled because the position of minimum c_p can move with the location of the shock which is more downstream for higher Mach numbers.

The end plate effect with its increase in pressure difference between left and right side of the VTP can be observed in Fig. 6, too. For the transonic flight conditions shown here this leads for all configurations except those of the VTP+fus with the lowest end plate effect to an exceedance of the critical Mach number and the occurrence of shocks.

3.1.4. Comparing VTP01 and VTP02

In the preceding paragraphs the effects which can be extracted from the subsonic and transonic pressure coefficient distributions were discussed. Now, in Fig. 7 the principal effect of the change in geometry between the two VTPs on the c_p- distribution is shown.

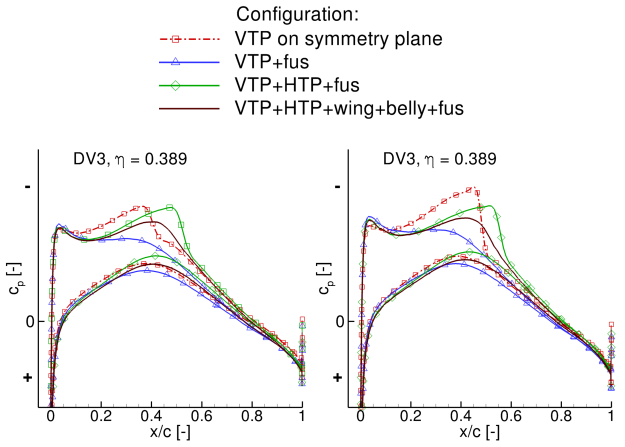

Fig. 7. Comparison of VTP pressure coefficient distributions at about 1/3 of VTP span (measured from root); δ_r = 0°, β = 2°, M = 0.85; left: VTP01, right: VTP02

While for the subsonic case the pressure coefficient distributions are very similar, i. e. the general appearance stays the same, more differences are visible for the transonic case. Due to the reduced sweep angle for VTP02 the impact of transonic effects is increased. This leads, as Fig. 7 shows, to an increase in shock strength and further downstream position of the shock. This agrees well with the description of the effects of sweep in the literature [12].

3.2. Surface Pressure Coefficient Distributions

Previously, section cuts illustrating the pressure coefficient were shown allowing a quantitative comparison at some distinctive locations along the VTP span. Now the pressure coefficient distributions are shown as a contour plot on the surface to give a more complete view, thus allow visualizing some further effects which are easier to recognize in this kind of presentation.

In Fig. 8 the surface pressure coefficient distribution of the VTP is shown for a high speed flight case with symmetric onflow conditions and zero rudder deflection. While VTP02 with reduced sweep angle is shown in this figure, the general effects for VTP01 are the same, but due to the increased sweep angle the minimum c_p-values are a bit reduced for that case.

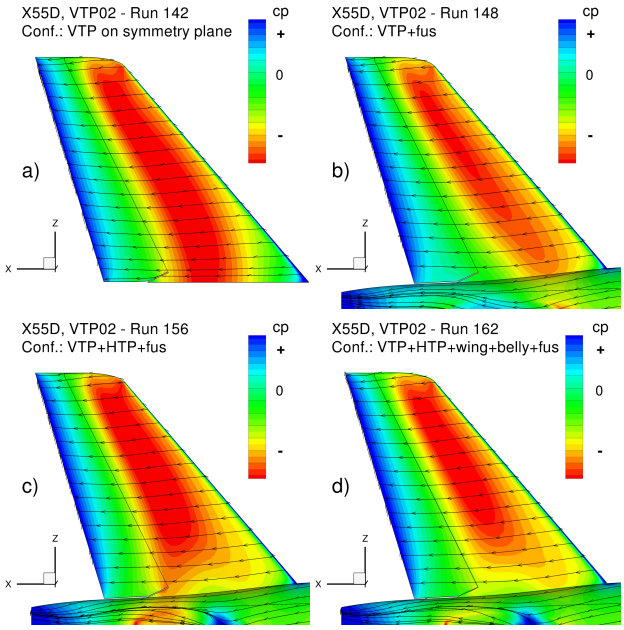

Fig. 8. VTP surface pressure coefficient distributions for symmetric flow conditions for all four configurations, δ_r = 0°, M = 0.85, VTP02

For the simplified configuration VTP on symmetry plane (Fig. 8 a, top left) the impact of the missing fuselage is clearly visible in the surface pressure coefficient distribution. Due to the missing fuselage its boundary layer is missing as well leading to more negative c_p-values extending up to the symmetry plane. On the other hand for the configurations with fuselage the boundary layer leads to a reduction in flow velocity and as a consequence in a less negative pressure coefficient towards the root of the VTP.

For the configuration VTP+fus (Fig. 8 b, top right) the change of c_p-distribution compared to the full configuration (Fig. 8 d, bottom right) especially in the area of the VTP root is visible. That is the impact of the missing HTP and wing. This is caused by the missing additional flow acceleration due to the presence of the HTP magnified by the change of the HTP flow field via a change in its angle of attack caused by the wing downwash.

For the configuration consisting of VTP, HTP and fuselage (Fig. 8 c, bottom left), the pressure coefficient on the VTP close to the HTP is more negative than in the case of the full configuration (Fig. 8 d). Thus the altered flow at the HTP due to the existence of the wing has a noticeable influence on the VTP c_p-distribution. The effect of the wing on the HTP is visualized in Fig. 9 for these two configurations and at the same flow conditions. Here one configuration without wing (VTP+HTP+fus) is compared to one with a wing present (full configuration – VTP+HTP+wing+belly+fus). The pressure coefficient distribution for a cut at the HTP near the fuselage shows that for the configuration without wing lift is created at the HTP. Adding just the wing results in a downforce there due to the downwash produced by the wing changing the onflow direction at the HTP.

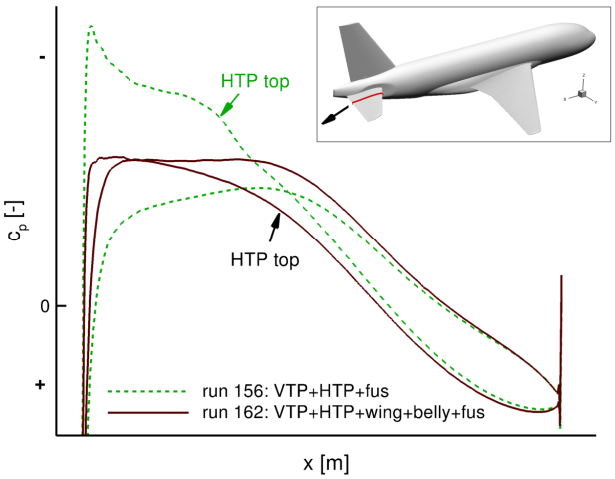

Fig. 9. VTP02: comparison of pressure coefficient at HTP cut near fuselage for conf. with and without wing, symmetric flow conditions, δ_r = 0°, M = 0.85

The effects described can be found in a similar way for the other flow cases investigated with unsymmetrical flow conditions where a sideslip angle β = 2° or a rudder deflection δ_r = -2° is present. This has an impact on the side force created and hence on the gradients calculated.

To summarize, essentially two effects have a main contribution, changing the pressure coefficient distribution as shown above. The first effect is the end plate effect described at the end of Section 3.1.1 above. The second is the change in geometry. The different parts of the aircraft mutually induce forces on each other, i. e. also on the VTP. The missing fuselage alters the flow as well as the missing HTP when comparing the simplified configurations to the most complete one. The effects described are magnified under transonic flow conditions.

3.3. Spanwise Local C_y Distribution

The distribution of the local side force coefficient C_y can be used here to highlight some interesting differences between the two VTP planforms and the repercussions originating in the simplification of the geometry. Because the strongest effect can be seen for the OEI design case due to the non-linear behavior of the VTP at the corresponding flow conditions, this case is chosen here as an example.

Before starting to discuss this, it is important to remember the difference between the circulation distribution (which is proportional to the lift distribution) and the local lift *coefficient* distribution. While the former is proportional to the load distribution and an important measure in judging the induced drag created by the wing, the latter is of interest when assessing the location of the onset of flow separation and the stall behavior. Both values are connected via the following simple formula for the case of the VTP, where C_y is equivalent to the local lift coefficient C_l at the wing, c(z) is the local chord along the VTP span, and Γ(z) is the local circulation:

$$\Gamma(z) \sim C_y \cdot c(z) \quad (6)$$

If one is accustomed to looking at the lift coefficient distribution of rather conventional wings with low sweep, combined with moderate aspect and taper ratio and maybe with some twist built in, one expects some approximation of an ellipsoidal shape. In that case, the maximum value of C_l is always located at or close to the root, with the result that the stall onset starts there. If we now take the case of a VTP like the ones presented in this paper, it is important to make oneself aware about the differences in planform characteristics and what this means for its aerodynamic behavior. First, a low aspect ratio tends to move the maximum of C_y towards the root. On the other hand, the large sweep angle and considerable taper combined with a symmetric airfoil without spanwise twist, tends to move the location of $C_{y,max}$ outboard. In the end, a side force coefficient distribution results which has its maximum at about 70% of the span, decreasing somewhat towards the root and more strongly towards the tip before ending with a local peak due to the acceleration caused by the flow around the tip. An example is shown in Fig. 10 where the local side force coefficient versus the dimensionless spanwise coordinate of the VTP η_V is depicted for a flight case with small sideslip angle and zero rudder deflection at low speed flight conditions.

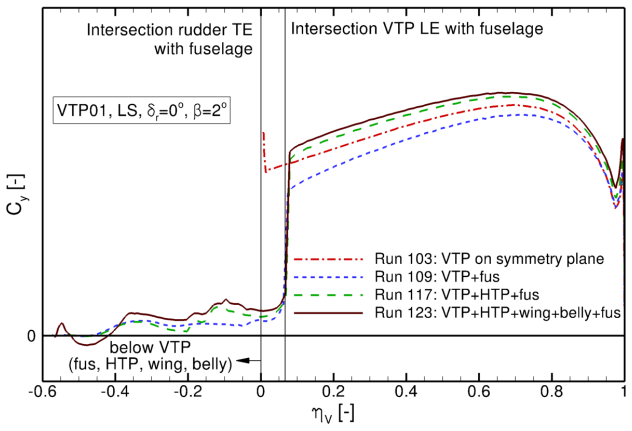

Fig. 10. Local side force coefficient versus the dimensionless spanwise coordinate of the VTP for all four configurations, δ_r = 0°, β = 2°, low speed, VTP01

If the angle of sideslip and/or the rudder deflection is now further increased, the curves presented in the diagram just mentioned at first simply stretch to achieve higher local C_y-values all along the VTP span. As soon as the maximum sustainable C_y is achieved somewhere along the span, the

flow starts to separate there. In case of a typical VTP as presented here, this happens somewhere around 70% of the chord. Going beyond that angle, the separation quickly moves towards the tip and then after that slowly towards the root. Different stages of this development are shown in Fig. 11 and Fig. 12 which depict the C_y-distribution for the two VTP's at a high rudder deflection angle of -35° and a moderate sideslip angle of 5° for the different simplification levels. The differences in the extent of the separated area are here caused by the level of simplification and the difference in sweep angle between the VTP's.

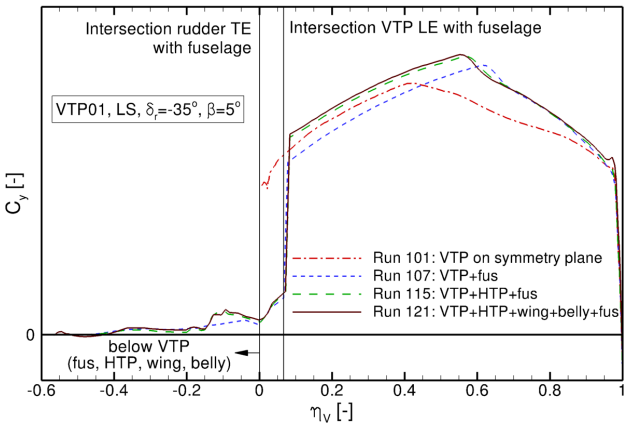

Fig. 11. Local side force coefficient versus the dimensionless spanwise coordinate of the VTP: for all four configurations, δ_r = -35°, β = 5°, low speed, VTP01

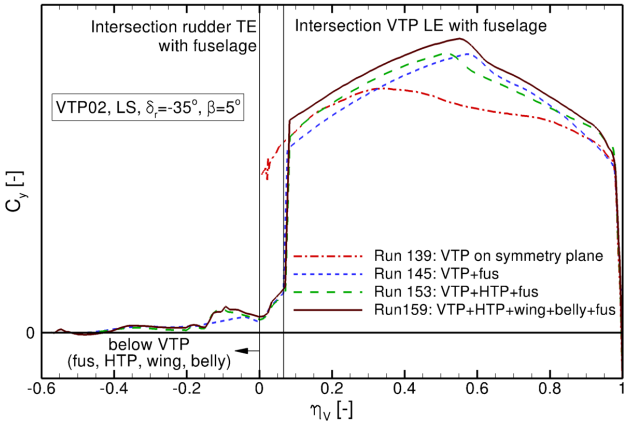

Fig. 12. Local side force coefficient versus the dimensionless spanwise coordinate of the VTP: for all four configurations, δ_r = -35°, β = 5°, low speed, VTP02

Common to both VTP planforms and all configurations, apart from VTP02 on the symmetry plane, is a pronounced maximum in C_y after a steep and almost linear rise from the root. Beyond the maximum towards the tip a reduction in local C_y can be noted, which results from the flow separation on the rudder between the location of $C_{y,max}$ and the tip. Looking at Fig. 13 this is supported by the presence of a noticeable peak in the c_p-distribution at the rudder hinge axis below the spanwise location of $C_{y,max}$.

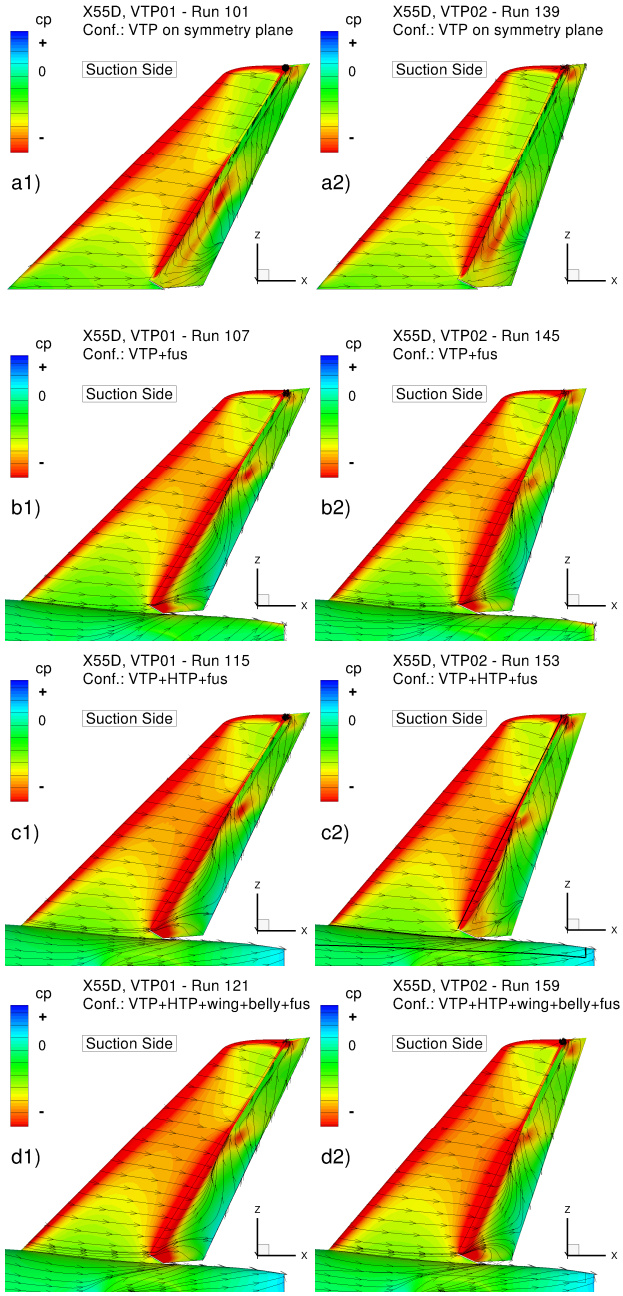

Fig. 13. VTP colored with surface pressure coefficient: all four configurations, δ_r = -35°, β = 5°, low speed, VTP01 (left) and VTP02 (right)

Discussing the influence of the simplification of the configurations first using VTP01 as an example, one notes that the rudder is separated to a larger extent for the configuration VTP on symmetry plane. The missing relief due to the influence of the fuselage boundary layer at the root and the fact that all root sections feature a full airfoil, leads to the situation that this configuration reaches stall onset conditions at lower sideslip angles and/or rudder deflections than the other three configurations. At the same values of δ_r and β as depicted in the diagram, $C_{y,max}$ of this configuration is therefore located closer to the root. Up to this maximum of C_y the shape of the C_y-distribution runs almost parallel to the other ones. The C_y-distributions of the three configurations including the fuselage have a rather similar shape, with the case without wing and HTP

having a somewhat lower $C_{y,max}$. This leads to a lower global value for the coefficient $C_{YV,OEI-DC}$, as can also be seen from the bar chart in Fig. 22, while the remaining two configurations have almost identical values.

Now switching to the explanation of the differences in characteristics between the two VTP planforms, the first what can be recognized is the fact that the configuration VTP on symmetry plane for VTP02 has an even earlier onset of separation. This is indicated by a more fully developed separation on the rudder as can be concluded from the somewhat smaller spanwise extent of a still noticeable c_p-peak at the rudder hinge line. A further indication is the fact that in Fig. 12 almost no part of the C_y-distribution is parallel to that of the other three configurations, not even close to the root. Also, while the two configurations including the HTP have an almost identical C_y-distribution in case of VTP01, this is no longer true for VTP02. The case without wing generates a considerably lower $C_{YV,OEI-DC}$, and the spanwise locations of $C_{y,max}$ have also moved apart between the two VTP's.

With all this in mind, it becomes clear that not only a modification of the planform changes the characteristics of the VTP (as intended), but also the level of simplification of the geometry – which is not intended. Considering an optimization as described in the introduction of this paper, this will most likely cause the optimization to take a different route should it be based on a simplified instead of the full configuration. If and how much this leads to a difference in the optimized VTP characteristics can of course not be answered with the data at hand.

3.4. Influence of the HTP-Induced Pressure Field on the VTP

The influence of the presence of the HTP and the HTP induced pressure field on the VTP pressure coefficient distribution was already discussed in some detail in the preceding Section 3.2. The first influence of the HTP on the VTP originates from the modification of the flow velocity in the vicinity of the tails due to the HTP's displacement effect. This basic effect can be magnified considerably by changes in the HTP's trim setting, but in most cases apart from very extreme ones will be an acceleration on the top side of the HTP.

What a major influence the presence of the HTP has on the VTP and its pressure coefficient distribution and in turn on the coefficients calculated for the VTP can be illustrated by the following example: The direct influence of the wing on the VTP is quite small, especially at flight conditions with a sideslip angle of about zero ($\beta \approx 0°$). The surface pressure coefficient distribution for a configuration with VTP+wing+belly+fus in Fig. 14, where the HTP is missing, looks about the same as the one for the configuration VTP+fus where HTP as well as wing and belly fairing are missing. The pressure distribution to compare would be the top right one (b) from Fig. 8. When comparing this configuration VTP+wing+belly+fus with the one where the HTP is present the corresponding c_p-distribution in the bottom right (d) of Fig. 8 results. Here, major changes in the lower part of the VTP can be noted. From that it becomes obvious, that the effect of the wing directly on the VTP is small, but quite pronounced in combination with the HTP.

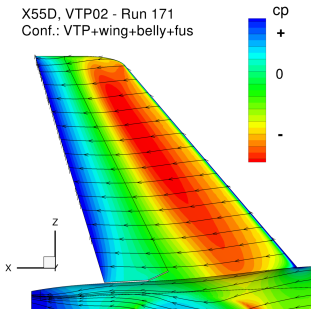

Fig. 14. VTP surface pressure coefficient distributions for symmetric flow conditions for configuration VTP+wing+belly+fus, $\delta_r = 0°$, high speed, VTP02

Since one major effect resulting from the presence of the wing is the change of the angle of attack of the HTP, a change in the HTP trim setting would have a comparable effect.

This influence is due to the close geometrical proximity of HTP and VTP as it can be found on a conventional rear end configuration. In addition the fuselage cross section becomes smaller towards the rear part of the aircraft, making the coupling between HTP and VTP even stronger. As visualized in Fig. 15 and Fig. 16 the leading edge of the HTP root is located a little distance in x-direction behind the location of the maximum thickness of the VTP for this aircraft. Here and in the rear part of the VTP the influence of the HTP is thus the strongest.

For the configuration VTP+HTP+fus without wing the angle of attack at the HTP is less negative compared to the configuration with wing since the downwash of the wing is missing. A negative angle of attack at the HTP leads to a downforce created there. Shifting this angle to a more positive onflow angle, the downforce is reduced and the HTP finally starts to produce lift. For reasons of trimming the aircraft the HTP usually creates a downforce.

A downforce at the HTP means that a more negative pressure is produced at its lower side which produces a stronger suction field there compared to the upper side of the HTP with higher, less negative pressure. A higher pressure there prevents in turn the VTP to get to such negative pressure as it would in case the HTP would not be there.

If the flight conditions are asymmetric, either due to $\beta \neq 0°$ or because the rudder of the VTP is deflected, the pressure field resulting at the left and right side of the HTP is asymmetric as well. This is due to the much less disturbed onset flow of the right HTP under this sideslip condition, where the flow is coming from the right. The left HTP, especially its root region, on the other hand, is located in a low-velocity zone caused by the presence of the large fuselage disturbing the flow there.

An example for such a case with sideslip angle from the right is shown in Fig. 15 for the configuration VTP+HTP+fus and in Fig. 16 for the full configuration for high speed flight conditions. Depicted is a cut through the left and right part of the HTP close to the fuselage as well as a pressure cut through the VTP close to the fuselage.

Here for the complete configuration (Fig. 16) a downforce is created at both sides of the HTP but on the right side the downforce is stronger. Due to the resulting higher pressure at the top of the right HTP, a higher, less negative pressure coefficient results at the right side of the symmetric VTP compared to the left side.

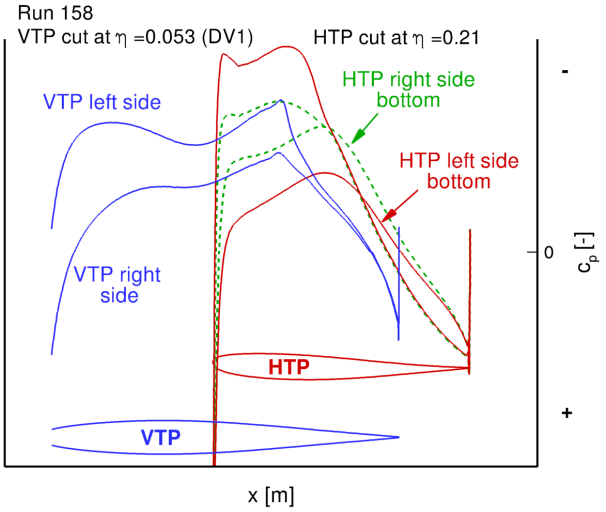

Fig. 15. Pressure coefficient distribution of the VTP and HTP with their relative position in x-direction to each other, configuration: VTP+HTP+fus, δ_r = 0°, β = 2°, high speed, VTP02

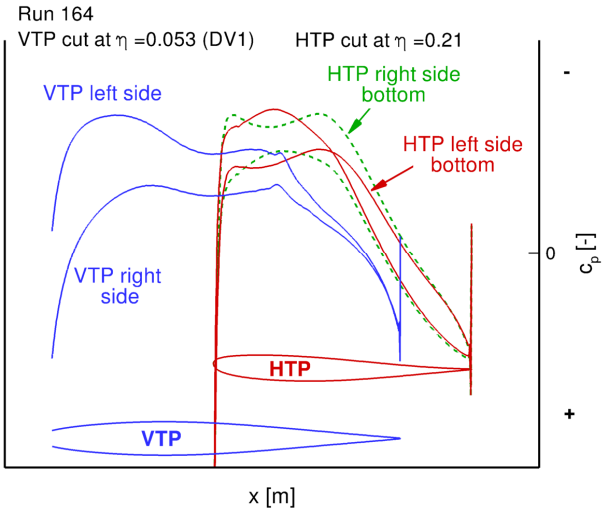

Fig. 16. Pressure coefficient distribution of the VTP and HTP with their relative position in x-direction to each other, full configuration, δ_r = 0°, β = 2°, high speed, VTP02

Turning now to Fig. 15 where the same configuration is shown but for the case without the wing, lift is created at both sides of the HTP. This downforce in the former case is now turned into lift due to the more positive angle of the flow approaching the HTP which is not redirected by the influence of the wing. Here the increased lift at the left HTP is caused by a higher suction there as on the right side of the HTP. This suction leads to a more negative pressure at this side of the VTP which is here more negative than for the configuration with wing. Clearly visible is the influence of the HTP related to its geometric position. The pressure coefficient of the VTP is influenced most at the location where the HTP has its pressure minimum.

Here it was just discussed what kind of influence the presence or non-presence of the HTP has on the pressure distribution of the VTP. In reality, the influences of the HTP can be even larger depending on the changes allowed for the VTP during an optimization. The relative location between HTP and VTP in x-direction, the HTP trim angle, the z-distance between HTP and VTP root, the location of the HTP in relation to the wing wake, the relation between HTP and VTP root chord length and probably more influences between HTP and VTP suggest quite a close dependency of one of them on the presence and characteristics of the other. Thus omitting the HTP would likely simplify the optimization target function quite considerably, with unknown consequences for the location and presence of local and global optima of the VTP characteristics.

4. DISCUSSION OF RESULTS REGARDING VTP OPTIMIZATION

In this chapter the coefficients and gradients listed in Section 2.1 are determined as described in Section 2.5. The results obtained for VTP01 and for VTP02 with a lower sweep angle are than compared. In a second step conclusions are drawn to answer the question, what impact the use of a simplified configuration would have if used for an optimization instead of the most complete configuration.

4.1. Analysis of Coefficients and Gradients

The coefficients and gradients for the high speed flight conditions are shown in Fig. 17 to Fig. 19, followed by those for the low speed flight conditions in Fig. 20 to Fig. 22. Each diagram shows the values of the coefficients and gradients for VTP01 and VTP02 and the difference between both for each configuration.

First some observations derived from comparing both VTP planforms are presented, followed by those related to the different configurations and their geometric simplifications. Here first the coefficients and gradients dependent on the side force are discussed followed by some remarks on the drag coefficient of the VTP.

4.1.1. Comparing VTP01 and VTP02

In general, it can be observed for high as well as for low speed flight cases, that the gradients and coefficients are higher for VTP02. This agrees well with theory where a decreasing sweep angle leads to an increase of the gradients [12]. The same was already observed for the pressure coefficient. Since the integration of the VTP pressure coefficient yields the side force which is used to calculate coefficients and gradients, this was to be expected. This increase of the coefficients and gradients for the most complete configuration can also be found for the simplified configurations. However, it has to be noted, that the magnitude of the increase is not the same as for the full configuration.

4.1.2. Comparing the Different Configurations

After looking at the differences of the two planforms in the last section, the focus in the following sections is on the differences in the aerodynamic characteristics between the four configurations of one VTP planform, caused by the different levels of simplifying the complete configuration. In order to highlight those quite noticeable differences, the selected coefficients and gradients will be discussed.

4.1.2.1. Configuration: VTP on symmetry plane

For the configuration VTP on symmetry plane it can be noted that the coefficients and gradients obtained, are smaller in magnitude than those of the complete configuration, except for the drag coefficient incurred at cruise flight conditions which is discussed later.

As explained in Section 3.3, the reason why $C_{YV,OEI\text{-}DC}$ is smaller for this configuration than for all other configurations is mainly due to the missing relief of the boundary layer and the fact that all sections are complete, leading earlier to a higher loading on the VTP, so that stall onset is reached at lower values of δ_r and/or β. This means that for any given value of rudder deflection and sideslip angle, the loss of side force due to the separated area is larger for this configuration than for all others.

Further observations regarding the other gradients and coefficients are made below during the discussion of the results for the other configurations.

4.1.2.2. Configuration: VTP+fus

For the next configuration VTP+fus it can be observed, that the same is true concerning the gradients and coefficients as for the VTP on the symmetry plane and that the values are smaller than those for the complete configuration. In fact, the gradients of this configuration VTP+fus are even smaller than those of the VTP on symmetry plane when looking at the high speed cases and on the gradient $C_{Y\delta r}$ for the low speed flight conditions. This is mainly due to the smaller end plate effect for the configuration VTP+fus which is indeed the smallest one for all configurations as explained in Section 3.1.1, where this effect was already noted while discussing the pressure coefficient distributions. For the high speed flight conditions this difference to all other configurations is quite visible since the resulting less negative pressure coefficient on the VTP for the configuration VTP+fus leads to the fact that no shocks occur while this is the case for the other configurations.

For the low speed flight conditions the situation that all gradients ($C_{Y\delta r}$ and $C_{YV\beta}$) are smaller for the configuration VTP+fus than for the isolated VTP is not found, since there are no dominating transonic effects. For the rudder efficiency at zero sideslip ($C_{Y\delta r}$), the origin of the side force generated is centered around the hinge line. In this case it seems that the existing boundary layer and the reduced end plate effect of the configuration VTP+fus compared to the configuration VTP on symmetry plane combine in such a way, that the force generated especially in the root region is considerably reduced. This results in the fact that the configuration VTP+fus has the lowest rudder efficiency.

For the VTP efficiency ($C_{YV\beta}$) resulting from a small sideslip angle on the other hand, the situation along the leading edge is of much greater importance. Here, the isolated VTP is at a disadvantage, because the additional acceleration due to the tapering of the fuselage and the flow over the fuselage top which appears curved in flow direction is missing. In the end this might be the reason for the fact, that the VTP efficiency is smallest for the configuration VTP on symmetry plane, resulting from local flow conditions at the root overpowering the global end plate effect. A contributing factor may also be the way the coefficients are calculated, which causes the VTP-induced side force on the fuselage to be attributed to the VTP itself as explained in more detail in the next section. This contribution is missing for the isolated VTP as the symmetry plane has no area where a sideways-directed force can develop.

4.1.2.3. Configuration: VTP+HTP+fus

For most of the gradients investigated, the configuration VTP+HTP+fus over-predicts the values of the most complete configuration or results in values of about the same level. As discussed in Section 3.2 the wing plays an important role here changing the angle of attack of the HTP which in turn changes the pressure distribution there. This again has an influence on the VTP pressure coefficient distribution, also described in Section 3.4. Without the change of the HTP angle of attack caused by the wing, a higher pressure difference of the left and right sides of the VTP is obtained, leading to an over-prediction of the side force compared to the complete configuration. The integrated values from the pressure coefficient distribution resulting in the side force can be compared directly to the respective gradient since all other values required for the determination of the gradient are constant.

When comparing the configuration VTP+HTP+fus to the two more simplified ones with the VTP on the symmetry plane and the VTP on the fuselage, one notes that the magnitude of the coefficients and gradients, except for the drag coefficient in cruise flight, is higher. It can be observed that the addition of the HTP to the configuration with fuselage and VTP leads to a remarkable difference.

This influence of the HTP can be explained when considering that the HTP contributes to the side force obtained at the VTP not only by increasing the end plate effect. To recall, in Eq. (4) it was said that the coefficient C_{YV} is obtained by subtracting the configuration without tails, i. e. without VTP and HTP, from the configuration including VTP (and HTP where present). Consequently, a side force component generated by the HTP also adds to this coefficient which has an influence on the coefficient for the simulated One-Engine-Inoperative design case $C_{YV,OEI\text{-}DC}$ and on $C_{YV\beta}$. Here the asymmetric flow conditions due to the sideslip in combination with the presence of the fuselage and HTP dihedral as well as sweep of the HTP play a role. Unequal forces on left and right HTP result, having a net component in y-direction due to the dihedral. This side force component adds to the level already generated by the VTP.

When discussing the pressure coefficient distributions in Section 3.1.1, the end plate effect was mentioned as having a major influence by leading to a higher aerodynamic aspect ratio and thus side force at a given angle of sideslip in the linear range. This effect is the highest for the isolated VTP calculated on a symmetry plane and leads to the high side force values generated by that configuration. However, the symmetry plane is flat and has no area towards the side like a fuselage where a pressure field and a side force can be created. This sidewise-directed force is partly induced by the VTP. Due to the way the coefficients are calculated, the part induced by the VTP is captured as well and is added to the side force coefficient of the VTP. In summary, this induced force created on the fuselage is higher than the decrease in side force due to the decreased aerodynamic aspect ratio compared to the VTP on the symmetry plane.

4.1.2.4. Configuration: VTP+HTP+wing+belly+fus

The addition of wing and belly fairing changes the flow field downstream and consequently also the onset flow conditions of the VTP. For the gradients at high speed conditions, this results in a decrease in the VTP's side force contribution for the full configuration while it stays at approximately the same level for the low speed conditions.

The main difference to the configuration VTP+HTP+fus is, as discussed earlier in Section 3.2, the changed angle of attack at the HTP. In addition, the presence of the wing introduces a new influence called "sidewash", which is only non-zero if the aircraft flies with a non-zero sideslip angle. Apart from that the same arguments are valid as for the configuration VTP+HTP+fus when comparing this most complete configuration to the simplified ones.

Interesting to note is the comparison between the configurations VTP+HTP+fus and the complete configuration for the coefficient $C_{YV,OEI\text{-}DC}$ with regard to the change between VTP01 and VTP02. While the value of this coefficient becomes slightly more positive when adding wing and belly fairing to the configuration using VTP01, the reverse is true for VTP02. In that case, the coefficient $C_{YV,OEI\text{-}DC}$ becomes more negative. This means that in this case, not even the trend between VTP01 and VTP02 is the same when switching between the simplification levels. A similar situation can be observed for $C_{Y\beta}$ for the low speed case.

4.1.2.5. Drag Coefficient Incurred at High Speed Conditions

The drag coefficient at cruise flight conditions, shown in Fig. 19, is increased for VTP02 compared to VTP01. This is mainly due to an increase in pressure drag. Because of the reduction of the quarter chord sweep angle the critical Mach number is reduced. The results are shocks which occur earlier or the strength of which is increased. This was visualized in the VTP section pressure coefficient distribution shown in Section 3.1.4. The resulting wave drag adds to the pressure drag.

Focusing again on the differences between the geometry simplifications it attracts attention that only three configurations are shown. Since the drag coefficient for the VTP is always calculated based on a HTP-off configuration in the context of this investigation as described in Section 2.5.4, the same result is obtained for the configurations VTP+fus and VTP+HTP+fus because without HTP both configurations are identical. Therefore only the configuration VTP+fus is shown in the diagram in Fig. 19.

For all simplified configurations the drag is overestimated compared to the full configuration. If a simplified configuration would be used for performing the drag assessment this would be more preferable to an underestimation, because the VTP does not seem to be better in terms of drag than it is. Nevertheless, the differences are quite high with values above 10% increase compared to the most complete configuration. Here, again the pressure drag is the part of the drag responsible for the differences. These large differences must arise from wing and belly fairing which are missing. Wing and belly fairing are located upstream of the VTP influencing the flow field behind them.

The cases considered here are for aircraft cruise conditions where transonic flow is prevalent. Over the wing, regions with supersonic flow exist which are terminated by shocks, leading to losses. These losses are due to friction (in the boundary layer) and due to the entropy increase over the shock. This reduces the kinetic energy of the flow and therefore the flow velocity further downstream, leading in turn to a decrease in local Mach number. Because of this, the Mach number in the region of the VTP span is reduced compared to the case without wing. This may be the reason for the smaller drag coefficient of the VTP, because a (partial) reduction in the VTP onset flow Mach number reduces the occurrence of shocks on the VTP and thus its drag increment.

4.2. Conclusions Regarding Optimization

For an optimization it would be beneficial to have a low number of grid points reducing time and cost for mesh generation and flow simulation. Since the mesh resolution of the VTP should not be reduced in order to reliably capture its aerodynamic characteristics, the question was raised whether the other parts of the aircraft geometry apart from the VTP are required for a numerical optimization.

When comparing the results of the two investigated VTPs VTP01 and VTP02 an increase in a coefficient for the complete configuration also leads to an increase in the same for the simplified configurations. But that fact alone is in the case of an optimization not sufficient if the results of the simplified configuration should be somehow transferable to the complete configuration to which the optimized VTP will be added in the end.

Now comparing the values of a coefficient for the geometry VTP01 with the alternative design VTP02, one notes that the absolute differences for a simplified configuration are not the same as for the complete configuration. This is visualized in Fig. 17 to Fig. 22 where the computed differences are given as the third bar for each configuration.

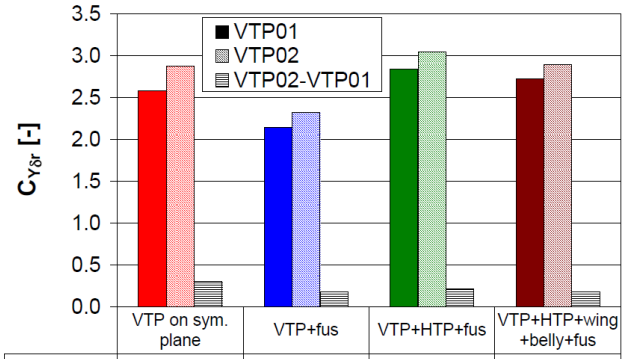

	VTP on sym. plane	VTP+fus	VTP+HTP+fus	VTP+HTP+wing +belly+fus
VTP01	2.57	2.14	2.83	2.72
VTP02	2.87	2.31	3.04	2.89
VTP02-VTP01	0.300	0.174	0.211	0.176

Fig. 17. Gradient $C_{Y\delta r}$ for the different conf's: Comparison VTP01 and VTP02; $\beta = 0°$, δ_r linear range, M = 0.85 (HS)

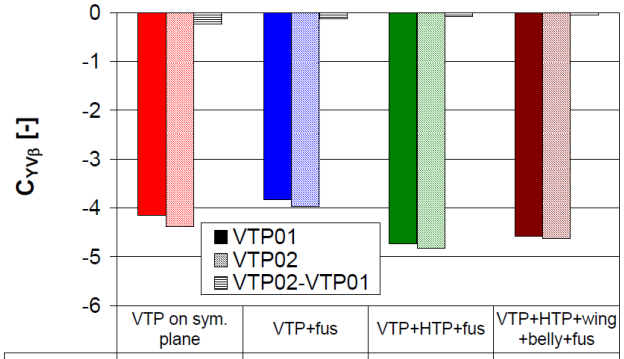

	VTP on sym. plane	VTP+fus	VTP+HTP+fus	VTP+HTP+wing +belly+fus
VTP01	-4.15	-3.84	-4.74	-4.58
VTP02	-4.38	-3.97	-4.82	-4.62
VTP02-VTP01	-0.234	-0.132	-0.085	-0.046

Fig. 18. Gradient $C_{Y\beta}$ for the different conf's: Comparison VTP01 and VTP02; $\delta_r = 0°$, β linear range, M = 0.85 (HS)

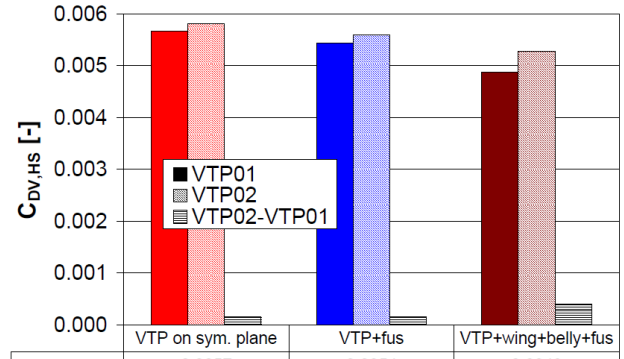

	VTP on sym. plane	VTP+fus	VTP+wing+belly+fus
VTP01	0.0057	0.0054	0.0049
VTP02	0.0058	0.0056	0.0053
VTP02-VTP01	1.525E-04	1.522E-04	3.953E-04

Fig. 19. Coefficient $C_{D,HS}$ for the different conf's: Comparison VTP01 and VTP02; $\beta = 0°$, $\delta_r = 0°$, M = 0.85 (HS); C_D(VTP on – VTP off) (HTP off for all calculations)

	VTP on sym. plane	VTP+fus	VTP+HTP+fus	VTP+HTP+wing +belly+fus
VTP01	2.00	1.85	2.09	2.09
VTP02	2.17	1.98	2.25	2.21
VTP02-VTP01	0.174	0.129	0.159	0.120

Fig. 20. Gradient $C_{Y\delta r}$ for the different conf's: Comparison VTP01 and VTP02; $\beta = 0°$, δ_r linear range, M =0.2 (LS)

	VTP on sym. plane	VTP+fus	VTP+HTP+fus	VTP+HTP+wing +belly+fus
VTP01	-3.21	-3.40	-3.88	-3.89
VTP02	-3.35	-3.47	-3.95	-3.93
VTP02-VTP01	-0.133	-0.071	-0.065	-0.043

Fig. 21. Gradient $C_{Y\beta}$ for the different conf's: Comparison VTP01 and VTP02; $\delta_r = 0°$, β linear range, M = 0.2 (LS)

	VTP on sym. plane	VTP+fus	VTP+HTP+fus	VTP+HTP+ wing+belly+fus
VTP01	-1.13	-1.29	-1.37	-1.36
VTP02	-1.14	-1.36	-1.38	-1.43
VTP02-VTP01	-0.012	-0.061	-0.015	-0.073

Fig. 22. Coefficient $C_{YV,OEI\text{-}DC}$ for the different conf's: Comparison VTP01 and VTP02; $\delta_r = -35°$, $\beta = 5°$, M = 0.2 (LS); C_Y(Tails on – Tails off)

Thus, when calculating the characteristics of the VTP based on a simplified configuration and an improvement is obtained, it cannot be concluded how large the improvement will be when determining the same based on the complete configuration. Since, as discussed before, non-linear effects play an important role for some characteristics, it might even be that there is no improvement at all. Also the effects observed between the configurations leading to a partly different flow behavior especially in the VTP root region, where the simplified geometry exhibits the largest changes compared to the complete configuration, are quite different and specific to the simplification used. Another example is the onset of separation on the rudder in the case of the coefficient $C_{YV,OEI\text{-}DC}$, where the changes between the simplification levels lead to a different behavior – compare the discussion in Section 3.3 about the spanwise local C_y-distribution.

In the end, the main conclusion is that no major simplification is allowable as soon as any coefficient which behaves in a non-linear way is concerned. It will be very difficult to prove this in a mathematical sense, but the fact nevertheless is quite obvious when looking for example at the very different shape of for example the pressure distributions resulting from the different levels of geometric simplifications in the transonic case. Arriving at the same optimized shape independent of the simplification level used would thus be purely coincidental.

Nevertheless it could be possible, that a simplified geometry leads to an optimized solution with a value of the objective function similar to the one which would be obtained with the complete configuration. However, this could only be checked by performing an optimization for each of the simplification levels and then comparing the results.

5. SUMMARY

With the long-term background scenario of a full multi-disciplinary tails optimization in mind, a pre-investigation was carried out for the aerodynamic part of the optimization using the VTP as an example. The objective was to assess whether one would obtain the same optimization result when performing the optimization with the VTP on the complete aircraft geometry compared to an optimization where parts or even everything but the VTP is removed in order to reduce time and cost for mesh generation and flow analysis.

In order to investigate this problem, two different VTP geometries called VTP01 and VTP02 were designed and analyzed. The difference between the two VTPs results from a reduction of the quarter chord sweep angle by five degrees, while all other geometric parameters were kept constant. For each of the two VTPs, four configurations with different simplification levels were investigated: The isolated VTP on a symmetry plane, the VTP on a fuselage, the VTP combined with HTP and fuselage and the most complete configuration with VTP, HTP, wing, belly fairing and fuselage. One set of VTP characteristics was derived from each of those simplification levels by calculating different coefficients and gradients for low and high speed flight conditions. Those values would be part of the objective function which needs to be defined for an actual optimization.

To facilitate an answer to the question posed initially, not only the raw values of the coefficients and gradients computed were considered, but an effort was also made to discuss and understand the effects which lead to the changes in the aerodynamic behavior between the geometric simplifications. From that it can be concluded, that the influence of the simplification of the geometry on the aerodynamic characteristics of the VTP and therefore also the resulting coefficients and gradients is quite strong.

With regard to an optimization the differences between the values obtained for two different VTP geometries are important. Here it was observed that this difference for a simplified configuration is not the same for the simplified configurations in comparison to the complete configuration. Hence, having obtained the results for a simplified configuration, it cannot be concluded how much the improvement will be for the complete configuration. If the performance of the VTP as installed on the aircraft shall be optimized, the other parts of the aircraft should not be neglected during the computations to assess its performance as part of the optimization process. If the optimization scenario includes any design variables which behave in a non-linear way, for example transonic effects and flow separation, these effects cannot be captured by adding a constant value or a multiplicative factor, but all factors causing this behavior have to be included during the computations.

A good example, because it can be easily followed, is the following: The wing downwash itself has only little influence on the characteristics of the VTP and thus it could be expected that there is little influence when the wing is removed. But close to the VTP the HTP is located, and its pressure field has a considerable influence on the VTP. The HTP in turn is directly influenced by the wing via its downwash, with the end result that a removal of the wing also has a remarkable influence on the VTP.

Concluding what was just summarized it can be stated, that an optimization based on a simplified configuration will likely lead to a different VTP shape than one done based on the complete aircraft configuration. Therefore, it seems that it is in general not advisable to heavily simplify the configuration to be optimized unless robust knowledge about the characteristics of the objective function is available in order to avoid detrimental effects on the optimization result obtained.

ACKNOWLEDGEMENTS

The authors would like to thank several colleagues from the Airbus department Aerodynamic Design Nose/Center Fuselage and VTP. Here Matthew Byrne from Salford University, Greater Manchester, deserves special mentioning, as it was him who generated all meshes for VTP02 and did the corresponding flow calculations during his internship at Airbus. The authors also would like to thank Erich Paul who was always available for advice and took the time to discuss the data analysis for many hours. Also to mention is Arne Grote who was a great help and always available for advice while setting up the CAD geometry.

REFERENCES

[1] Gebhardt L., Enk S., Weber C., Brezillon J.: Numerical Optimization on the Vertical Tailplane of Transport Aircraft, executed as part of the LuFoIV Research Project AeroNext+. Presentation 16th DGLR Fach-Symposium of STAB, RWTH Aachen (2008)

[2] Kröhnert A., Gebhardt L.: Investigation of the Impact of Simplifying the Aircraft Geometry on the Characteristics of the Vertical Tailplane. Proceedings STAB 2010, Logenhaus, Berlin, Nov. 9-10 (2010)

[3] Pettersson K., Rizzi A.: Reynolds Number Effects Identified with CFD Methods Compared to Semi-Empirical Methods. ICAS 2006-2.3.4, pp. 14 (2006)

[4] Flores R., Ortega E., Oñate E.: Numerical Investigation of Wind-Tunnel Model Deformations Caused by the Twin-Sting Support System. J Aircr., 47:708-714, doi: 10.2514/1.45272 (2010)

[5] Chen B.H., Wellmer G., Ballmann J.: Numerical Prediction of Aeroelastic Effects on Twin-Sting-Rig mounted Models for Rear Fuselage and Empennage Flow Investigations in Transonic Wind Tunnel. International Forum on Aeroelasticity and Structural Dynamics (2007)

[6] CentaurSoft Homepage: http://www.centaursoft.com, Cited 10 June 2012

[7] Deutsches Zentrum für Luft- und Raumfahrt e.V.: Technical Documentation of the DLR TAU-Code. Technical Report, Institute of Aerodynamics and Flow Technology, DLR Braunschweig/Göttingen (2006)

[8] Gerhold T.: Overview of the Hybrid RANS Code TAU. In: Kroll N., Fassbender J. (ed): MEGAFLOW – Numerical Flow Simulation for Aircraft Design. Notes on Numerical Fluid Mechanics and Multidisciplinary Design 89:81–92. Springer (2005)

[9] Horlings H.: Staying Alive with a Dead Engine. Paper presented during the European Aviation Safety Seminar of the Flight Safety Foundation, Athens, Greece (2006). Source: http://www.avioconsult.com

[10] Rotta J.: Luftkräfte am Tragflügel mit einer seitlichen Scheibe. Ingenieur-Archiv, Band XIII, Heft 3, pp.119-131 (1942)

[11] Thomas F.: Grundlagen für den Entwurf von Segelflugzeugen. Motorbuch Verlag, Stuttgart (1984)

[12] Anderson J.D. Jr.: Aircraft Performance and Design. McGrawHill, ISBN D-07-116010-8 (1999)